A Model of Tectonic Stress State and Rate Using Northridge Aftershocks

Susanna Gross
Cooperative Institute for Research in the Environmental Sciences, University of Colorado, Boulder

April 7, 2000

Abstract

A model of the spatial and temporal distribution of seismicity both before and after the Northridge, California earthquake has been used to estimate the background stress state, loading rate, and some parameters relating to fault friction. A detailed source model was used to calculate the stress change field from the Northridge mainshock, which was fit to the spatial distribution of seismicity. Agreement between the best-fitting background stress state from seismicity modeling and the background stress state inferred from focal mechanisms was found to be 99% significant, showing that the spatial distribution of seismicity contains information about the stress state. The stress rate found for the Northridge area, $\approx$ 1.2 Pa/day (0.004 bar/a), is approximately a factor of 9 less than the stress rate expected from observed strain rates, which implies that aseismic deformation is reducing seismic hazard in the Los Angeles basin. The resulting estimate of the friction parameter $A_D \approx 0.008$ is similar to laboratory values if an effective normal stress much smaller than the overburden and similar to background stress magnitudes $\sigma \approx 70$ MPa from the seismicity modeling is assumed to apply. Estimates of the magnitude of background stress, gradient of stress with depth and effective coefficient of friction are quite uncertain.

1 Introduction

One of the current seismological problems of greatest relevance to society concerns seismic hazard associated with blind thrust faults in the Los Angeles, California basin. Recent studies of strain rates across the basin (Dolan *et al.* 1995) suggest that larger and more destructive earthquakes than any in the historical record could occur. Geologic cross-sections of the basin (Huftile and Yeats, 1996) indicate several large low angle faults which could rupture in rare large magnitude events that would be devastating to the 14 million inhabitants of the greater Los Angeles metropolitan area. The high observed strain rate and low seismicity of the basin (Dolan *et al.* 1995) need not necessarily be due to overdue large earthquakes. Aseismic deformation could accommodate a significant proportion of the strain. The thickness of the seismogenic layer and the geometry of active faults within it are also not completely known, and are important for any accurate estimate of seismic potential.

The Northridge earthquake of 1994 both illustrated the significant seismic hazards associated with blind thrust faults near Los Angeles and provided a means to examine them. Studies of the event detail its tectonic context (Hauksson *et al.* 1995), source properties (Wald *et al.* 1996), basin structure (Pujol, 1996), and the engineering consequences (Chang *et al.* 1996). The aftershock sequence was well recorded and active enough to permit studies of variations in focal mechanisms of the aftershocks (Zhao *et al.* 1997). Hardebeck and Norris (1996) showed that the aftershocks of the Northridge earthquake have focal mechanisms that match the postseismic stress field more often than the background seismicity does, but when revising the work Hardebeck *et al* (1998) found that the Northridge aftershock mechanisms were not significantly different than mechanisms from a randomly distributed set of control events. Stein *et al.* (1994) have shown that the spatial distribution of Northridge aftershocks is correlated with the stress change field from the Northridge source - providing more evidence that static stresses do influence the spatial distribution of aftershocks.

In this work, estimates of the rate of accumulation of stress in the Los Angeles basin are derived from the spatial and temporal distribution of Northridge aftershocks. The technique builds upon previous work in which it was assumed that aftershocks are triggered by changes in the static stress field. Stress rates are useful for hazard assessment because they are more directly related to the accumulation of elastic energy released in earthquakes than strain rates are. Strain my be released aseismically. The technique used was first introduced in a study of the Landers earthquake (Gross and Kisslinger 1997) and then applied to the Loma Prieta earthquake sequence (Gross and Bürgmann 1998). Stress rates for Landers and Loma Prieta derived from seismicity illustrate that the technique produces results comparable to estimates derived from strain observations and consistent with tectonic interpretations. The technique is also sensitive to the release of stress that occurs near creeping faults. Background stress states derived from the spatial distribution of seismicity are consistent with focal mechanisms, and suggest that the technique is providing independent information about the stress field, because no focal mechanisms are used in the inversion.

2 Data

The seismicity catalog used for this work was produced by the California Institute of Technology in cooperation with the United States Geological Survey (Wald *et al.* 1994). The catalog was limited to events given quality letter 'A', for the most accurate locations, and only included events with hypocenters between 33.5° and 35° north latitude and 117.5° and 119.5° west longitude. Blasts as defined by the Caltech blast catalog were eliminated. For much of the work, no magnitude cut was applied, since completeness is not required for the stress state modeling. Time limits were chosen so that there would be nearly 10,000 events defining the background seismicity, and 10,000 events after the mainshock. The catalog used for stress modeling without magnitude or depth cuts began in June 1932 and ended in June 1998. A longer catalog running through the end of 1999 was used to define the temporal decay of the Northridge aftershocks. Subsets of the catalog limited to events deeper or shallower than 9 kilometers, or magnitudes $M_L > 1.5$ were defined and used in stress and stress rate inversions to assess how much the results depend upon variations in the catalog. Real physical variations in stress state are expected for the depth subsets, but not for the magnitude cut subset. The sub-catalogs had fewer events and the fits are therefore not as well constrained. For the stress rate calculations based on subsets of the catalog, events before 1980 were eliminated, making the data more homogeneous, and the seismicity rate more stable. A special catalog which omitted all events closer to the source than 5km was constructed and analyzed for a test of the influence of near-source aftershocks on the solution.

Another input piece of information essential to the models constructed in this paper is the source model of Wald *et al.* (1996), derived from a combination of strong motion, teleseismic, GPS and leveling data. This model includes 196 fault patches with sides 1.7 and 1.3 kilometers long and ranging in depth from 5 to 20 kilometers. All the fault patches have a strike of 122° and a dip of 40°, but the rakes are variable. To compute stress fields, the fault patches were represented with dislocations of equivalent area, moment and mechanism, embedded in a 3D elastic half-space. Singularities in the stress field on the fault were removed by omitting sources less than two kilometers from the point at which the stress was being computed. Stresses were computed using formulas due to Okada (1992).

3 Analysis

3.1 Overview of the Method

The stress state and rate analysis technique employed in this work includes several different kinds of modeling and classes of results. Relationships between the elements of the method are depicted in the flowchart, Figure 1. Catalog hypocenters and the source model constrain the background stress state and fault friction model. The stress state model may be tested by comparing the result with inversions based upon focal mechanisms, because no focal mechanisms are involved in the inversion. Stages of the analysis involving Dieterich (1994) seismicity theory are represented by shaded boxes on the figure. The stress state inversion is not shaded because it employs the much less restrictive assumption that aftershocks should be more abundant in source volumes with increased failure stress, and does not use the timing of events. Estimates of stress rate do depend indirectly upon rate and state dependent friction, because they are based upon a relationship between stress step and number of aftershocks which is derived below from Dieterich's (1994) aftershock decay relation. Similarly, the estimate of aftershock duration t_a may not be used to estimate a value of the friction parameter A_D without Dieterich (1994) seismicity theory.

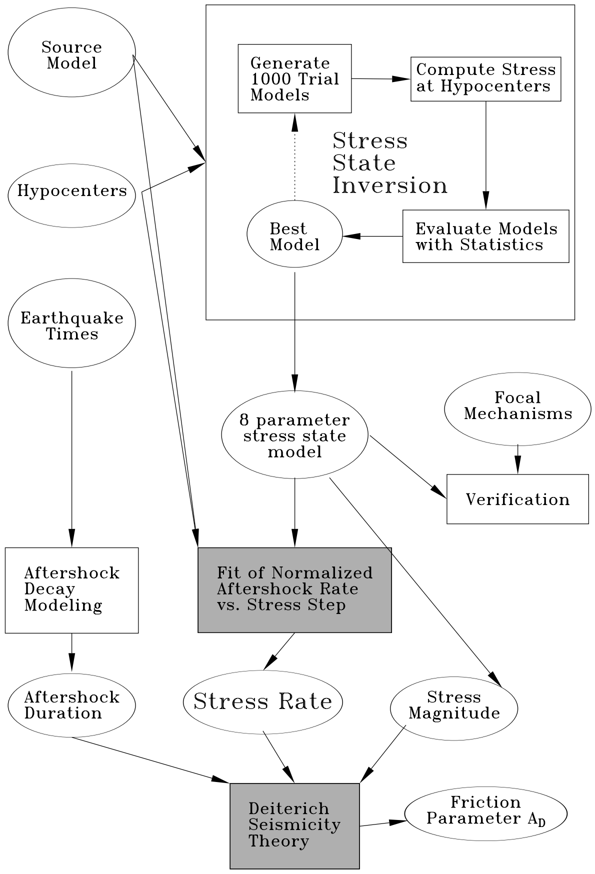

Figure 1: This flowchart illustrates model parameters (circles) and analysis procedures (boxes) involved in the stress state and rate modeling. Shaded boxes represent analysis dependent upon Dieterich (1994) seismicity theory, and arrows indicate the direction of information flow. Times and magnitudes of earthquakes are not used in the stress state inversion except to define aftershock and background periods.

3.2 Stress Modeling

The stress modeling technique presented in Gross and Kisslinger (1997) was updated and employed

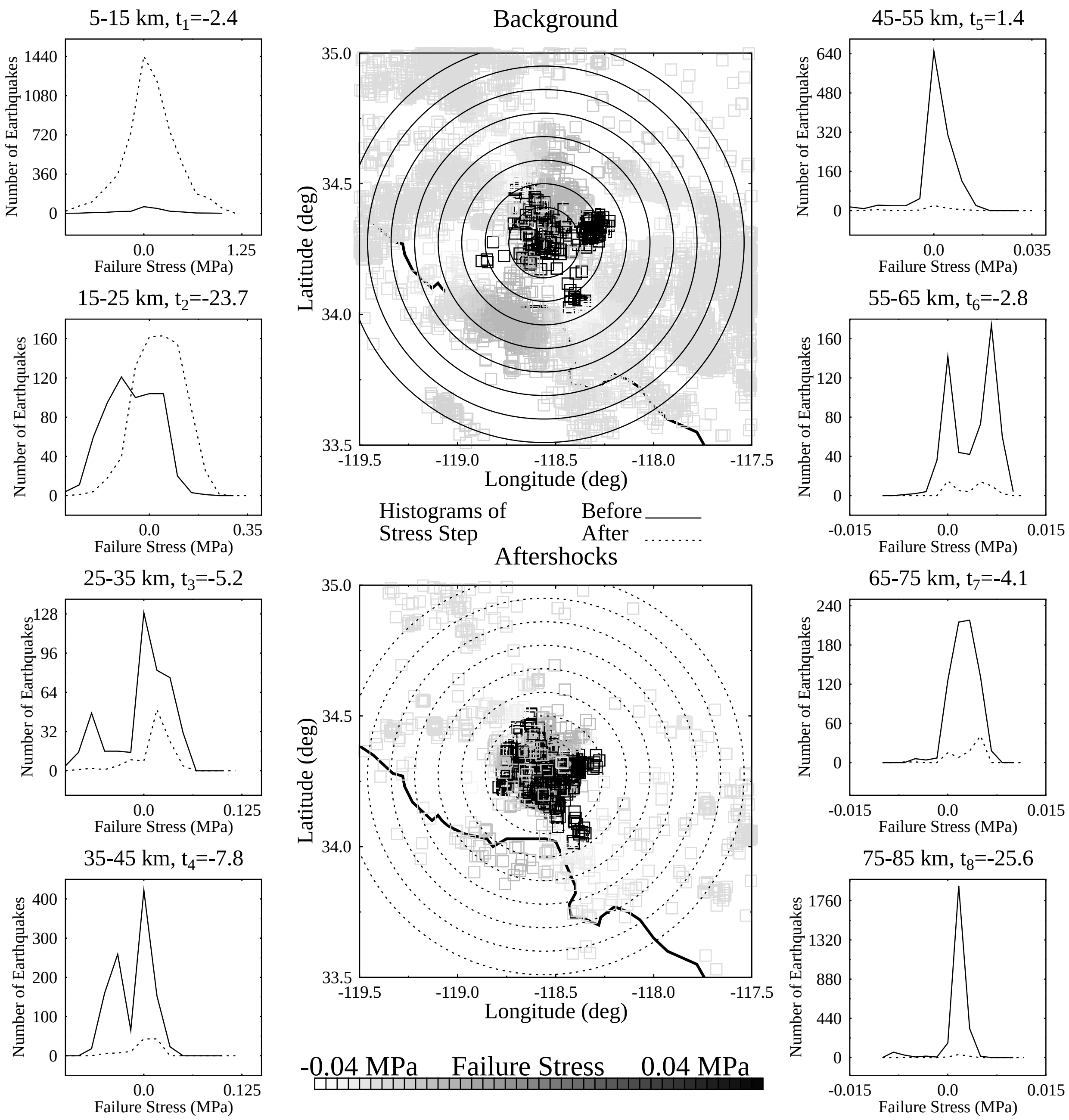

Figure 2: The central figures show seismicity in map view, with darker shades indicating increases in failure stress for the model listed in the first line of Table 1. The solid and dotted lines on the histograms plotted on this figure illustrate the distributions of change in failure stress on optimally oriented planes, $\Delta\sigma_F$ for seismicity taken from different distance ranges surrounding the hypocenter of the Northridge mainshock before and after the mainshock. T-statistics are computed for each distance range to test how well the change in seismicity correlates with the change in stress, and those t-statistics are summed to evaluate the models. Thousands of models are compared by computing t-statistics for each one.

in this work and is summarized as follows: The stress step from the mainshock is used to compute failure stress, and the background stress state is fit to the spatial distribution of seismicity. Eight free parameters defining the background stress are chosen in order to make the failure stress at hypocenters of aftershocks greater than the failure stress at hypocenters of background seismicity.

Stress decreases are assumed to suppress seismic activity and stress increases are assumed to enhance it. The failure stress σ_F on optimally oriented planes is computed from the principal stresses σ_i, (including background stresses) and the effective coefficient of friction μ', which includes any effects of fluid pressure,

$$\sigma_F = \left(\sqrt{\mu'^2 + 1}\right)\left\{\frac{\sigma_1 - \sigma_3}{2}\right\} + \mu'\frac{\sigma_1 + \sigma_3}{2}. \quad (1)$$

This expression for failure stress is derived in the appendix. The failure stress σ_F is similar to the Coulomb Failure Function or CFF (Reasenberg and Simpson, 1992, King *et al.*, 1994, Harris and Simpson. 1996, Nostro *et al.* 1997), with the only significant difference being that we consider oblique slip when searching for the greatest failure stress. The effective coefficient of friction is sometimes written in terms of μ, the intrinsic friction coefficient and B, Skempton's coefficient,

$$\mu' = \mu(1 - B)$$

but Skempton's coefficient is an unknown function of fluid pressure, stress history, fault geometry and sealing, as difficult to determine for active faults as μ. The symbol $\Delta\sigma_F$ has been chosen to avoid the incorrect implication that the definition of failure stress involves an assumption of Coulomb friction, with frictional properties independent of time. The failure stress is a weighted sum of maximum shear and normal stress, with the effective coefficient of friction determining the relative effectiveness of normal and shear stresses in triggering aftershocks. Changes in failure stress $\Delta\sigma_F$ are found for each hypocenter by subtracting σ_F without the mainshock stress step from σ_F with it, $\Delta\sigma_F \equiv \sigma_F^{\text{total}} - \sigma_F^{\text{background}}$.

The best-fitting effective coefficient of friction μ' is not the same as the intrinsic friction μ measurable in the laboratory, because intrinsic friction coefficients are the ratio of total shear τ to effective normal stress $\sigma - P_f$ necessary to initiate slip on a surface. The effective coefficient of friction μ' is proportional to the local slope of the failure envelope, largely independent of the total pore pressure, but sensitive to changes in pore pressure inside the fault that may accompany steps in normal stress. If the failure envelope is a straight line and there are no changes in pore pressure, effective friction μ' and intrinsic friction μ will be equal. If pore fluids change in pressure by an amount identical to the step in normal stress, the effective coefficient of friction μ' will be zero.

3.3 Rate and State Dependent Friction

If a population of faults loaded by a long-term steady tectonic stressing rate $\dot{\sigma}_F$ and normal stress σ, so that it produces a rate of background seismicity r, is subjected to a step in stress $\Delta\sigma_F$, the new seismicity rate n will follow the following function of time t Dieterich (1994):

$$n = \frac{r}{\left[\exp\left(\frac{-\Delta\sigma_F}{A_D\sigma}\right) - 1\right]\exp\frac{-t}{t_a} + 1}. \quad (2)$$

A_D is a unitless proportionality factor relating friction to velocity, and

$$t_a = \frac{A_D\sigma}{\dot{\sigma_F}} \quad (3)$$

is the time at which the aftershock sequence approaches the steady background rate of seismic activity. These expressions were originally written with the assumption that the normal stress in the experiment is held constant, but Dieterich (1994, equation 9) does develop an expression for the evolution of the state variable that shows that changes in normal stress have the same effect as changes in shear stress, but with a different weighting. Gross and Kisslinger (1997) have identified the weighted sum of shear and normal stress with the failure stress σ_F, and have consequently written the rate and state equations in terms of $\Delta\sigma_F$.

At $t << t_a$ the Dieterich aftershock decay function reduces to a form very similar to the modified Omori model Utsu, (1961),

$$n = \frac{K}{(t+c)^p}. \tag{4}$$

In this expression, K controls the total number of aftershocks, c is a time shift that removes the singularity at $t = 0$, and p is decay exponent which typically has a value between 0.5 and 2, with $p = 1$ for the Dieterich (1994) decay function.

To compare the observed rates of activity with the Dieterich model, integrate the expression for n above from time 0 to some finite final time T, assumed much greater than c,

$$\begin{aligned} N &= K\ln(c+t)|_0^T, \\ &= K\ln(c+T) - K\ln(c), \\ &\approx K\ln(T) - K\left[\ln(t_a) - \frac{\Delta\sigma_F}{A_D\sigma}\right], \\ \frac{N/T}{r} &\approx \frac{1}{T}\frac{\Delta\sigma_F}{\dot{\sigma_F}}, \end{aligned} \tag{5}$$

because the mainshock recurrence interval is much longer than the aftershock duration or observation interval, $\Delta\tau/\dot{\tau} >> T$ or t_a.

Two crucial properties of Dieterich (1994) friction are the linear proportionality between the steady-state rate of seismicity and background stress rate, and a similar linear proportionality between the number of aftershocks and the stress step.

3.4 Objective Function

To quantify the fit of stress step to the spatial distribution of seismicity I compute:

$$\mathbf{t} = \frac{\overline{\Delta\sigma_F^{\text{before}}} - \overline{\Delta\sigma_F^{\text{after}}}}{\sqrt{s^2_{\text{before}}/N_{\text{before}} + s^2_{\text{after}}/N_{\text{after}}}}, \tag{6}$$

where the symbol s is used to represent the standard deviation of a set of $\Delta\sigma_F$ values, N the number of events in the set, and $\overline{\Delta\sigma_F^{\text{before}}}$ is the average change in failure stress evaluated at hypocenters of events that occurred before the mainshock. A t-statistic is computed from the seismicity from each of eight spherical shells shown in Figure 2. The summary statistic $\Sigma\mathbf{t}$ is defined to be the sum of t-statistics from the eight spherical shells, and it is this summary statistic which is used to select the best-fitting model. It should be noted that there is no expectation that events before the mainshock will be influenced by it. It is essential to compute $\overline{\Delta\sigma_F^{\text{before}}}$ in order to compare $\overline{\Delta\sigma_F^{\text{after}}}$ with it. The seismicity distribution is very strongly influenced by the distribution of active faults in the area, and that is why aftershocks cannot be interpreted without considering the locations of background seismicity.

Each stress state is defined by giving the orientations of the principal stresses in terms of the azimuth (az) of the most compressive principal stress (σ_1) (row 2 in Table 1), the plunges (pl) of the greatest and least principal stress (rows 3 and 5 in Table 1), and the ratio of stress magnitudes (row 6)

$$\phi = (\sigma_2 - \sigma_3)/(\sigma_1 - \sigma_3). \tag{7}$$

A new parameter r listed in row 7 defines the magnitude of the intermediate principal stress,

$$r = \sigma_2/\sigma_3. \tag{8}$$

The magnitude of the greatest principal stress (row 4) is taken negative in compression and is an effective stress, including the effects of pore

Table 1: Northridge Stress State Fits

	fixed	whole	M_L >1.5	dep<9km	dep>9km	dist>5km
$\Sigma\mathbf{t}$	-51	-54	-57	-41	-59	-50
σ_1 az	(13)	28±8	28±14	25 ±6	26 ±5	10±3
σ_1 pl	(-8)	-17±2	-20±6	-15±2	3±31	-37±27
σ_1 MPa	-94±15	-29 ±7	-14±5	-109±13	-53±15	-122±12
σ_3 pl	(80)	72±2	70±2	73±0.5	80±30	-11±54
ϕ	(0.22)	0.00±0.4	0.00±0.4	0.99±0.17	0.04±0.16	0.3±0.3
r	0.17±0.11	0.00±0.06	0.00±0.13	0.03±0.05	0.00±0.3	0.6±0.3
μ'	0.24±0.13	0.74±0.13	0.99±0.14	0.9±0.8	0.99±0.14	0.20±0.02
ρ'	-78±29	0.02±18	0.0±3.6	-51±7	2.3±2.6	-17±3
RMS	0	11	13	9	10	43

Numbers in parenthesis were constrained to match the stress state of Hauksson (1990), to which all the models were compared using the RMS. The RMS is the root mean square misfit for the angles: σ_1 azimuth, σ_1 plunge and σ_3 plunge.

pressure. Remaining parameters are the effective coefficient of friction μ', (row 8 and equation (1)), and the effective overburden density ρ' (row 9), which controls how quickly the vertical effective normal stress increases with depth. The first row in Table 1 gives the summary statistic $\Sigma\mathbf{t}$, which is the measure used to define how well the models fit in relation to one another. More negative numbers indicate better fits, but direct comparisons of summary statistics can only be made between models of the same catalog.

Summary t-statistics for 20,000 models were evaluated in the search for the best fitting model for the each of the cases listed in Table 1 with 8 parameters. Models are evaluated in 20 groups of 1000 each. The initial model parameters are uniformly and randomly distributed over a physically reasonable range for all of the parameters except the stress magnitude. Trial background stress magnitudes are uniformly distributed in logarithm of stress, with values ranging from 1 MPa to 1 GPa. After the first 1000 models have been evaluated, later trial parameters are drawn from distributions centered upon the best value found so far. The recently improved inversion method is a variation on a genetic algorithm, in which the offspring inherent a blend of characteristics from each parent, and the weighting between parents is the same for all parameters. This distributes the offspring on a line segment between the end points which represent the parents in parameter space. This kind of inheritance is most appropriate for geophysical problems in which the parameters depend upon one another. In the optimization carried out for this paper, only the best 100 models were combined to produce each new generation, and all the combinations were made with the best model found so far in the optimization. This is similar to the the inheritance found in a herd of deer, in which the dominant buck sires all the offspring. Half of the models were produced by mutations of the best model, using a triangular distribution whose half-width was equal to the maximum variation of the 100 best models in each parameter separately. The genetic algorithm automatically searches the best-fitting parts of model parameter space, finding the best model more quickly and more dependably than the previous inversion method. In order to verify that the inversions were not being caught in local minima and define the uncertainties they were each carried out 100 times.

3.5 Aftershock Decay Modeling

A method for fitting the Dieterich decay relation to the temporal decay of the aftershocks is needed in order to calculate t_a from the Dieterich model and derive a value of the friction parameter A_D using (3). A practical technique for fitting and comparing aftershock models having a variety of functional forms has been developed (Gross, 1996; Gross and Kisslinger, 1994; Kisslinger, 1993; Ogata 1983). This technique finds the best-fitting model by minimizing the Akaike information criterion (AIC), which also maximizes the likelihood of the model given the data.

For an aftershock model having n_p free parameters and a modeled rate $n(t_i)$, as a function of the time of the ith aftershock, the AIC is

$$\min(\mathrm{AIC}) = 2N - 2\sum_{i=1}^{N} \max[\log(n(t_i))] + 2n_p, \tag{9}$$

where N is the total number of aftershocks observed. The two models fit in this work (equations (2) and (4)) both have $n_p = 3$ free parameters, K, c and p for the Modified Omori model, and t_a, r and $-\Delta\sigma_F/A_D\sigma$ for the Dieterich model. Combining data with various $\Delta\sigma_F$ should not impair our ability to estimate t_a, since t_a is independent of stress step. The minimization is carried out by using the technique described by Gross (1996). The lowest minimum from a series of 20 downhill simplex runs is selected, with each run started from a different, randomly selected set of initial parameters. The last 10 runs are started progressively closer to the best value found so far.

4 Results

4.1 Estimating Stress State

Numbers listed in Table 1 describe the best-fitting background stress states and effective coefficients of friction for 6 different fits of the stress states to the seismicity distribution. Different catalogs were used for all of the cases except the first two. The first case listed in the table is constrained to match the stress state Hauksson (1990) inverted from focal mechanisms of earthquakes occurring in the Los Angeles basin before the Northridge earthquake. This background stress state is also used as a standard of comparison for the calculation of RMS misfits in the last row of the table. The RMS summarizes the differences between three angles defining the orientation of the greatest principal stresses, the azimuths and plunges in Table 1. Since the constrained fit is forced to agree with the result from focal mechanisms, its RMS is zero. The RMS misfits range in value from 9 to 43 degrees, with the greatest agreement with focal mechanisms found for shallow seismicity and the largest misfit for the inversion which omits seismicity near the fault. It appears that near source seismicity is an important contributor to the model.

The uncertainties quoted in the table were estimated by repeating the inversions 100 times for each case. The best-fitting model, based upon the summary statistic, is listed for each case, but the standard deviations are computed from the scatter of the 100 models about their average.

Figure 3 summarizes the background stress state inversions from both focal mechanisms (Hauksson 1990) (triangles) and the spatial distribution of seismicity (Table 1, circles). The shaded symbols near the center of the plot represent the nearly vertical least principal stress axes σ_3, and the black symbols show orientations of the greatest principal stress axes σ_1. Both methods have been applied to various subsets of the data,

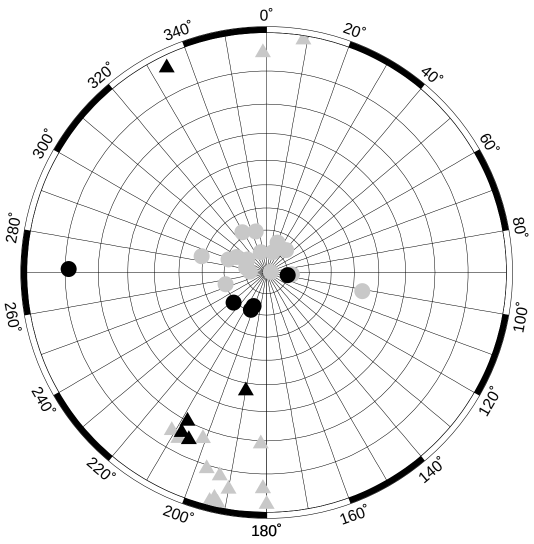

Figure 3: This lower hemisphere projection of modeled principal background stress axes shows orientations of least principal stress σ_3 in circles, and the greatest principal stress σ_1 in triangles. The grey symbols are from inversions of focal mechanisms, (Hauksson 1990), and the black symbols are from models of the spatial distribution of seismicity, also listed in Table 1.

showing some variations in stress state, but the two classes of models are reasonably consistent with one another.

Catalogs of synthetic aftershocks were created and modeled in order to evaluate the effectiveness of the stress modeling. These catalogs were based upon the spatial distribution of background seismicity, which was grouped into clusters defined with single link cluster analysis (Davis and Frohlich, 1991). Single link cluster analysis groups all events closer than a given distance and time separation, and merges clusters that have any common members. The distance and time thresholds are 10 kilometers and 10 days, respectively. Synthetic catalogs were created by including clusters with a probability inversely proportional to the number of events in each cluster. The simulated catalogs are quite similar to the original seismicity, but they may lack larger sequences or have multiple copies of them. Synthetic aftershocks were created by making the probability of including a cluster decrease with the third power of distance from an array of source points, with clusters closer than 10 kilometers from the source treated as if they were all at 10 kilometers distance. These simulated aftershocks are similar to natural aftershocks in their rate of occurrence as a function of distance (Figure 4), but they do not contain any information about the background stress field other than the source geometry. The synthetic catalogs also do not contain any temporal information beyond the definition of background and aftershock periods, because times are not used in the stress state inversion.

Synthetic aftershocks were used to evaluate the statistical significance of the fits listed in Table 1. Since the synthetic seismicity has the same chance of including rare large sequences as the natural data, the synthetic inversions provide a measure of how strongly large earthquake sequences influence the answers. The synthetic aftershocks do not contain any true stress transfer effects, only aftershocks in proximity to the mainshock. Inversions for background stress based upon synthetic data are a good measure of how successful such inversions could appear without any true effect of static stresses upon the seismicity. Tests of synthetic stress inversions were carried out with 100 different synthetic aftershock sequences, each generated from the un-cut catalog and Wald *et al.* (1996) source geometry. Each synthetic catalog was modeled in exactly the same way as the real data, with a best-fitting background stress state and effective coefficient of friction found. RMS misfits were computed for all of the cases, and found to average 116° with a standard deviation of 25°. No cases had an RMS smaller than the 11° RMS from the real data, which implies that the agreement between the background stress derived from seismicity and the background stress derived from focal mechanisms is approximately 99% significant.

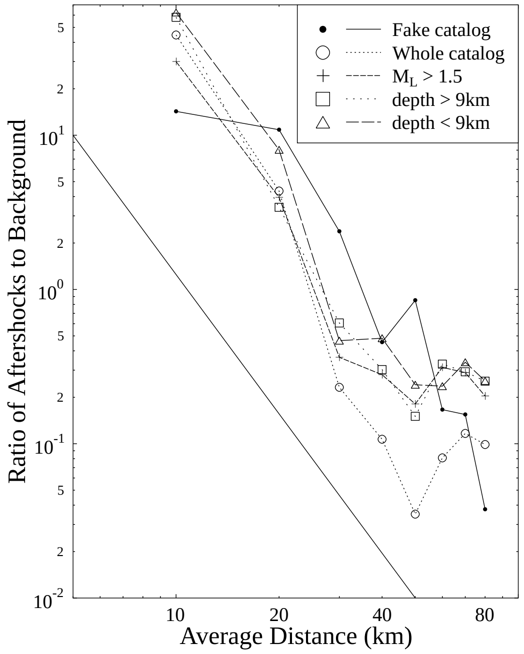

Figure 4: This scatter plot shows how the ratio of aftershocks to background activity decays with distance from the source. The straight line is the cube of distance decay expected for aftershocks triggered by static stresses.

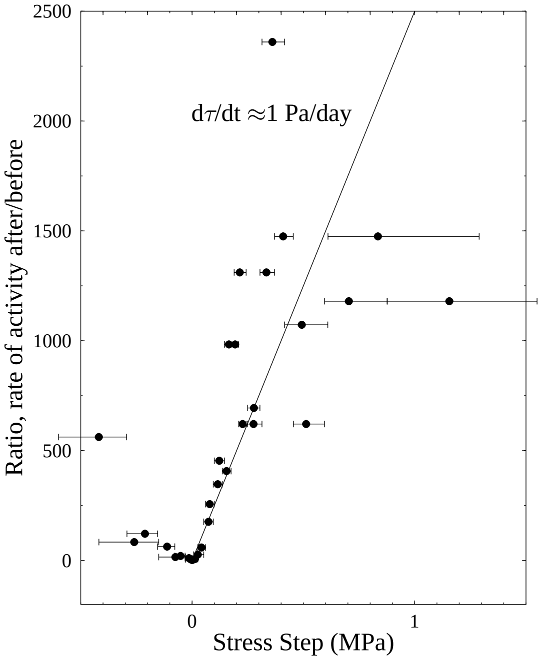

Figure 5: A scatterplot of aftershock amplification factor versus stress step shows an approximately linear trend expected from Dieterich (1994) seismicity theory, and allows rough estimates of loading rate to be made.

4.2 Estimating Stress Rate

Figure 5 illustrates how stress rates may be estimated from the variation of aftershock amplification with stress step. Aftershock amplification is the ratio of aftershock rate to background rate for a catalog subset. Catalog subsets have been defined in terms of their failure stress step, $\Delta\sigma_F$, which amounts to a special kind of spatial cut applied to both background and aftershocks. Equation 5 can be used to derive a stress rate from these data. The larger the stress step from the mainshock $\Delta\sigma_F$, the more aftershocks N we expect to see triggered, but triggering is also proportional to the rate of background seismicity r that occurs in an area, and inversely proportional to stress rate. To estimate the stress rate, I estimate the slope s of a line fit to a plot like Figure 4 and compute $\dot{\sigma}_F = 1/sT$.

Table 2 summarizes stress rate estimates made for Northridge using various catalogs and background stress states. The cases in the table are also listed in Table 1, with the best fitting background stress state derived from each catalog also used to define subsets of events with various stress steps. There are two types of estimates, based upon least-squares fits and L1-norm robust fits, which are supposed to be more resistant to outliers. Generally, there is less scatter in the robust estimates, which range

Table 2: Northridge Stress Rate Fits

Catalog	least squares	robust
constrained	6.1 +- 1.9 Pa/day	0.74 Pa/day
whole set	6.1 +- 3.6	2.2
M>1.5	4.2 +- 4.1	1.7
depth>9km	-0.6 +- 2.5	0.56
depth<9km	-1.5 +- 0.8	0.85
dist>5km	0.7 +- 0.5	0.95

from 0.56 Pa/day (0.002 bar/a) to 2.2 Pa/day (0.008 bar/a), and average to 1.2 Pa/day (0.0044 bar/a). These stress rates are quite low when compared to strain rates estimated for the Los Angeles basin. Huftile and Yeats (1996) estimated a convergence rate of 5mm/a across the Northridge thrust based upon a balanced cross section across the fault which is 38 km long. The strain rate across the section is 1.3×10^{-7} per year, and would require a shear modulus of 3.3×10^9 Pa, in order to be consistent with the stress rate. This shear modulus is roughly a factor of 9 smaller than typical values.

4.3 Aftershock Duration and the Friction Parameter

The final quantity that may be estimated from the Northridge sequence is the friction parameter A_D, which scales the direct effect of velocity upon friction. The observed aftershock decay can be fit by the Dieterich aftershock decay relation (2), which includes the parameter $t_a = A_D\sigma/\dot{\sigma_F}$. Figure 6 shows the aftershock decay from a catalog running through 1999, limited to $M_L > 1.5$ events whose stress steps were greater than the median for the aftershocks. The background rate was computed by applying the same magnitude and stress step cuts to the background time period, and it illustrates the overall very low level of background activity in the Northridge source region. Because the sequence lasts so much longer than the catalog, estimates of the background rate r'=0.192 events per day and aftershock duration t'_a=2847 days based solely upon the aftershock data are very inaccurate, but their product is quite well determined. A more accurate estimate of t_a can be found by combining the product $t'_a \cdot r'$ with the seismicity rate observed during the background period r=0.0011 events/day,

$$t_a = t'_a r'/r, = 497,794 \text{ days} = 1362 \text{ years}.$$

When combined with a value for the effective overburden pressure σ, the aftershock duration can be used to derive an estimate of the friction parameter A_D. If we assume a value of $\sigma \approx 70$ MPa, taken from the average magnitude of background stress in the stress state inversions, the estimate of A_D, is

$$A_D = \frac{t_a \dot{\tau}}{\sigma} \approx \frac{(1362 \text{ yr})(427 \text{ Pa/yr})}{(70 \text{ MPa})} \approx 0.0083,$$

which is between the value of $A_D \approx 0.02$ appropriate for hydrothermal conditions and the value appropriate for dry rock $A_D \approx 0.005$ (Dieterich, 1994). Alternatively, if an effective overburden is estimated from the density of the rock,

$$\sigma \approx (2600 \text{ kg/m}^3)(9.8 \text{ m/s}^2)(9000 \text{ m}) \approx 230 \text{ MPa},$$

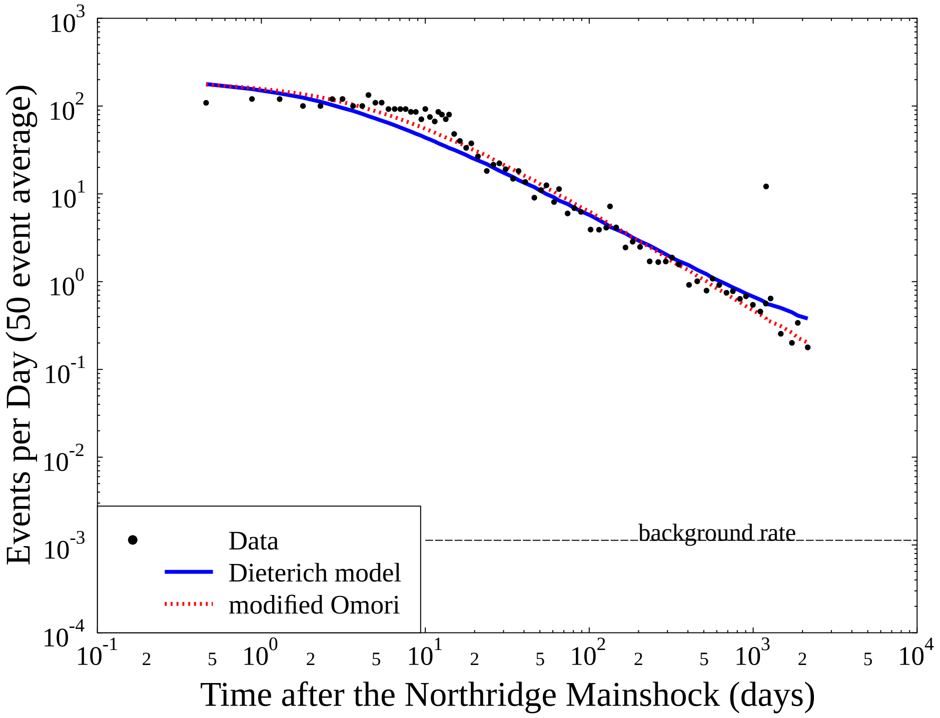

Figure 6: The rate of Northridge aftershocks is averaged over 50 events and plotted versus logarithm of time along with two aftershock decay models.

and the estimate of $A_D \approx 0.002$ is smaller than the smallest experimental values for dry rocks $A_D \approx 0.005$.

5 Discussion

The results above fairly firmly establish that the spatial distribution of seismicity can provide information about the stress state, in agreement with stress inversions based upon focal mechanisms, but there are many other quantities estimated as part of the technique which are less testable and more interesting. Some of the quantities are unstable, because inversions with slightly different catalogs produce significantly different results, and in some cases repeated inversions using the same data are not consistent. The effective coefficient of friction μ' and effective overburden density ρ', are unstable and therefore unreliable. The magnitude of the effective background stress fluctuates widely, averaging to 70 MPa, a value considerably lower than the overburden pressure. The effective coefficients of friction are also quite variable, and average to 0.67. The only effective coefficient of friction similar to intrinsic friction values is the one computed from the whole catalog.

Even though the stress rate estimates utilize a stress step model, they show less fluctuation and would appear to be determined to within a factor of 4. However, the inconsistency of the stress rate estimated in this work with strain rates observed in the same area suggest that extra skepticism is warranted when interpreting these results. These stress rate estimates should be used to suggest new avenues of inquiry, not form the basis of vital engineering decisions. Stress rates derived from a similar study of the 1992 Landers aftershocks (Gross and Kisslinger, 1997) were more consistent with known tectonic patterns, showing much greater loading rates along the San Andreas fault than the Mojave desert, but again the stress rate estimate for the Mojave was somewhat less than geodetic observations suggested it should be. When this analysis was applied to the 1989 Loma Prieta earthquake (Gross and Bürgmann 1998), stress rates fully consistent with geodesy were found, with reduced stress near the creeping section of the San Andreas fault. It is quite possible that the stress rate estimates presented here for the Los Angeles basin are correct. The disagreement with geodesy could be due to aseismic release of strain or to an unusually low shear modulus in parts of the basin, but the question is by no means resolved. Structures with unusually low shear modulus could have a large effect on the relationship between stress and strain rates in the area, but also be volumetrically insignificant and have little effect upon seismic wave propagation.

The estimate of friction parameter A_D is very uncertain, not least because it is difficult to establish what the effective normal stress is on buried faults. The estimate inherits uncertainties in the stress rate estimate which have just been discussed, as well as uncertainties in the aftershock duration t_a. Estimated values of A_D are strongly dependent upon the choice of catalog subset, because larger spatial subsets include many more background events than aftershocks, and this leads to much lower values of A_D. It is interesting that values consistent with the laboratory are found when low effective overburden pressure is assumed, because that is consistent with results reported for Loma Prieta and Landers, as well as the low background stress magnitudes in the stress state estimates. Together, the results suggest that deviatoric stresses are small, with horizontal principal stresses nearly equal to the vertical stresses.

The stress state inversion involves too few parameters to allow horizontal principal stresses to increase with depth. All changes in the stress state with depth are mapped into the single effective density parameter, controlling the increase in overburden. An effective density of zero implies that the relative magnitudes of the principal stresses are not changing with depth, in spite of the increasing overburden, and this means that the horizontal stresses must be increasing. Negative values of the effective density means that the horizontal stresses increase more rapidly than the vertical does. The low coefficient of friction found in some of the inversions can be interpreted as being consistent with pore fluids trapped within the faults. If these fluids increase in pressure by an amount equal to the increase in normal stress due to the mainshock, then the usual effect of increased normal stress could be masked, producing very low apparent coefficients of friction.

6 Conclusions

- The best-fitting background stress state from seismicity modeling is similar to the background stress state inferred from focal mechanisms, with a degree of similarity that occurs by chance approximately 1% of the time.

- Stress rates found for the Northridge area, ≈ 1.2 Pa/day, are much less than the rate expected from observed strain. Seismic hazard in the Los Angeles basin may be less than expected based upon strain rates, but this conclusion requires farther testing before it can be trusted.

- The estimate of $A_D \approx 0.008$ is similar to laboratory values if we assume an effective normal stress much smaller than the overburden and similar to background stress magnitudes from the seismicity modeling.

Appendix: derivation of σ_F

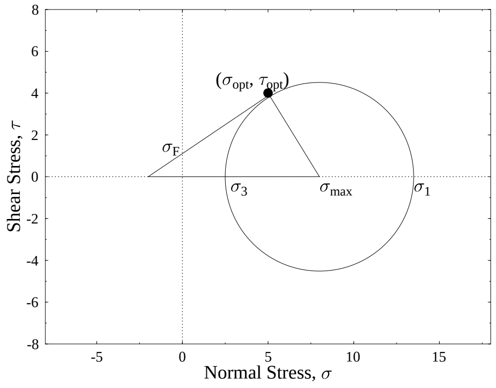

Figure 7: This cartoon of a Mohr's circle and linear failure envelope is used in the derivation of σ_F, the failure stress.

The failure function σ_F, shown on Figure 7, is the shear stress at which a failure envelope, assumed to be a line with slope μ', passes through the tau axis, where normal stress is zero. In the conventional representation, this intersection is written down in terms of $\tau_{\rm opt}$ and $\sigma_{\rm opt}$, which are the values of shear and normal stress (taken positive in compression) on optimally oriented planes. The stresses $\tau_{\rm opt}$ and $\sigma_{\rm opt}$ are found on the plot at the point where the failure line lies tangent to Mohr's circle. The failure line crosses the tau axis a distance $\mu'\sigma_{\rm opt}$ below $\tau_{\rm opt}$, so the failure stress may be written

$$\sigma_F = \tau_{\rm opt} - \mu'\sigma_{\rm opt}.$$

This formula has been presented by many authors (i.e., Reasenberg and Simpson, 1992; King *et al.*, 1994; Harris *et al.*, 1995; Nostro *et al.* 1997). The difficulty with it is that the optimal orientation for failure generally must be found before $\tau_{\rm opt}$ and $\sigma_{\rm opt}$ can be evaluated. For the stress modeling presented in this paper, as well as Gross and Kisslinger (1997), a different formula is used. This other formula for σ_F is equivalent to the above formula, but is written in terms of the maximum shear stress $\tau_{\rm max}$ and the normal stress on planes of maximum shear, $\sigma_{\rm max}$, which can easily be evaluated,

$$\sigma_F = \sqrt{1+\mu'}\tau_{\rm max} - \mu'\sigma_{\rm max}.$$

This expression can be derived from the simple Mohr circle with a straight failure line having slope μ', shown on Figure 7. Consider the right triangle, formed by the failure line, the σ axis, and the radius which runs from the tangent point to the circle's center. The hypotenuse of this triangle has a total length

$$\frac{\sigma_F}{\mu'} + \sigma_{\rm max},$$

because the triangle extends a distance σ_F/μ' beyond the τ axis. The circle radius is equal to $\tau_{\rm max}$, so the sine of the angle between the failure line and the horizontal axis can be written

$$\sin\alpha = \frac{\tau_{\rm max}}{\sigma_F/\mu' + \sigma_{\rm max}}.$$

The failure line has slope μ', so the sine of the angle it makes with with a horizontal line is

$$\sin\alpha = \frac{\mu'}{\sqrt{1+\mu'^2}}.$$

Substituting this into the previous expression and rearranging gives

$$\sigma_F = \sqrt{1+\mu'^2}\tau_{\rm max} - \mu'\sigma_{\rm max}.$$

When evaluating the expression in a three-dimensional stress field, it is necessary to solve for the principal stresses by diagonalizing the stress tensor, and then selecting the greatest and least principal stresses to compute the maximum shear stress $\tau_{\rm max} = (\sigma_1 - \sigma_3)/2$ and the normal stress on planes of maximum shear $\sigma_{\rm max} = (\sigma_1+\sigma_3)/2$,

$$\sigma_F = \left(\sqrt{\mu'^2+1}\right)\left\{\frac{\sigma_1-\sigma_3}{2}\right\} - \mu'\frac{\sigma_1+\sigma_3}{2}. \tag{10}$$

Writing the failure stress in terms of principal stresses makes it clear that ambiguities in the optimally oriented plane cannot contribute to uncertainties in the failure stress, because all optimal planes experience the same failure stress.

Acknowledgments: This work was supported by NSF EAR-9628458 and NASA NAG5-5168. Helpful reviews were provided by Carl Kisslinger, Roger Bilham, Ruth Harris, and Nick Beeler. Seth McGinnis provided his C-library implementation of Okada's equations for stresses and displacements due to a dislocation in an elastic halfspace.

S. J. Gross Cooperative Institute for Research in the Environmental Sciences, University of Colorado, Boulder, Campus Box 216 Boulder, CO 80309-216, (e-mail: sjg@quake.colorado.edu)

7 References

Chang, S. W., J. D. Bray, and R. B. Seed, (1996), Engineering implications of ground motions from the Northridge earthquake, *Bull. Seism. Soc. Am., 86,*, S270-S288.

Davis, S. D., C. Frohlich, (1991), Single-link cluster analysis of earthquake aftershocks decay laws and regional variations, *J. Geophys. Res., 96,* 6335-6350.

Dieterich, J. H., (1994), A constitutive law for rate of earthquake production and its application to earthquake clustering, *J. Geophys. Res.*, *99*, 2601-2618.

Dolan, J. F., Sieh, K., Rockwell, T. K., Yeats, R. S., Shaw, J., Suppe, J., Huftile, G., and Gath, E., (1995), Prospects for larger or more frequent earthquakes in the Los Angeles metropolitan region, *Science*, **267**, 199-205.

Gross, S. J. and R. Bürgmann, (1998), Rate and state of background stress estimated from the aftershocks of the 1989 Loma Prieta, California, earthquake, *J. Geophys. Res.* **103**, 4915-4928.

Gross, S. J. and C. Kisslinger, (1997), Estimating tectonic stress rate and state with Landers aftershocks, *J. Geophys. Res., 102*, 7603-7612.

Gross, S. J., (1996), Aftershocks of nuclear explosions compared to natural aftershocks, *Bull. Seismol. Soc. Am.*, *86*, 1054-1060.

Gross, S. J., and C. Kisslinger, (1994), Tests of models of aftershock rate decay, *Bull. Seismol. Soc. Am. 84*, 1571-1579.

Hardebeck, J. L. and J. J. Norris, (1996), A quantitative investigation of the static stress change model of earthquake triggering for aftershock sequences, EOS, Trans. AGU, 77(46), Fall Meet. Suppl. F482.

Hardebeck, J. L, J. Nazareth and E. Hauksson, (1998) The static stress change triggering model: Constraints from two southern California aftershock sequences, *J. Geophys. Res., 103*, 24427-24437.

Harris, R. A. and R. W. Simpson, (1996), In the shadow of the great 1857 Ft. Tejon earthquake - the effect on subsequent earthquakes in southern California, *Geophys. Res. Lett., 23*, 229-232.

Harris, R. A., R. W. Simpson, and P. A. Reasenberg, (1995), Influence of static stress changes on earthquake locations in southern California, *Nature, 375*, 221-224.

Hauksson, E., L. M. Jones, K. Hutton, (1995), The 1994 Northridge earthquake sequence in California: Seismological and tectonic aspects. *J. Geophys. Res., 100,* 12,335-12,356.

Hauksson, E. (1990), Earthquakes, faulting, and stress in the Los Angeles Basin, *J. Geophys. Res., 95,* 15,365-15,394.

Huftile, G. J., and R. S. Yeates, (1996), Deformation rates across the Placerita (Northridge $M_W = 6.7$ aftershock zone) and Hopper Canyon segments of the Western Transverse Ranges deformation belt, *Bull. Seism. Soc. Am., 86,* S3-S18.

King, G. C., R. S. Stein, and J. Lin, (1994), Static stress changes and the triggering of earthquakes, *Bull. Seismol. Soc. Am.*, *84*, 935-953.

Kisslinger, C., (1993), The stretched exponential function as an alternative model for aftershock decay rate, *J. Geophys. Res.*, *98*, 1913-1922.

Nostro, C., M. Cocco, and M. E. Belardinelli, (1997), Static stress changes in extensional regimes: An application to southern Apennines (Italy), *Bull. Seismol. Soc. Am., 87*, 234-248.

Ogata, Y., (1983), Estimation of the parameters in the modified Omori formula for aftershock sequences by the maximum likelihood procedure, *J. Phys. Earth*, *31*, 115-124.

Okada, Y., (1992), Internal deformation due to shear and tensile faults in a half-space. *Bull. Seism. Soc. Am., 82*, 1018-1040.

Pujol, J., (1996), An integrated 3D velocity inversion - Joint hypocentral determination relocation analysis of events in the Northridge area, *Bull. Seism. Soc. Am., 86,*, S138-S155.

Stein, R. S., G. C. P. King, J. Lin, (1994), Stress triggering of the 1994 M = 6.7 Northridge, California, earthquake by its predecessors, *Science, 265*, 1432-1435.

Wald, D. J., T. H. Heaton, and K. W. Hudnut, (1996), The slip history of the 1994 Northridge, California earthquake determined from strong-motion, teleseismic, GPS, and leveling data, *Bull. Seism. Soc. Am., 86,* S49-S70.

Wald, L. A., S. Perry-Huston, and D. D. Given, (1994), The southern California Network bulletin, January-December 1993, *U.S. Geol. Surv. Open File Rep., 94-199*, 1-56.

Utsu, T., (1961), A statistical study on the occurrence of aftershocks, *Geophys. Mag.*, **30**, 521-605.

Zhao, D., H. Kanamori, and D. Wiens, (1997), State of stress before and after the 1994 Northridge earthquake, *Geophys. Res. Lett., 24*, 519-522.